Calculations of subsonic and supersonic turbulent reacting mixing layers using probability density function methods

B. J. Delarue and S. B. Pope
Sibley School of Mechanical and Aerospace Engineering, Cornell University, Ithaca, New York 14853

(Received 7 January 1997; accepted 13 October 1997)

A particle method applying the probability density function (PDF) approach to turbulent compressible reacting flows is presented. The method is applied to low and high Mach number reacting plane mixing layers. Good agreement is obtained between the model calculations and the available experimental data. The PDF equation is solved using a Lagrangian Monte Carlo method. To represent the effects of compressibility on the flow, the velocity PDF formulation is extended to include thermodynamic variables such as the pressure and the internal energy. Full closure of the joint PDF transport equation is made possible in this way without coupling to a finite-difference-type solver. The stochastic differential equations (SDE) that model the evolution of Lagrangian particle properties are based on existing models for the effects of compressibility on turbulence. The chemistry studied is the fast hydrogen–fluorine reaction. For the low Mach number runs, low heat release calculations are performed with equivalence ratios different from one. Heat release is then increased to study the effect of chemical reaction on the mixing layer growth rate. The subsonic results are compared with experimental data, and good overall agreement is obtained. The calculations are then performed at a higher Mach number, and the results are compared with the subsonic results. Our purpose in this paper is not to assess the performances of existing models for compressible or reacting flows. It is rather to present a new approach extending the domain of applicability of PDF methods to high-speed combustion. © *1998 American Institute of Physics.* [S1070-6631(98)00302-X]

I. INTRODUCTION

The interest in high-speed combustion, as, for example, in SCRAMJET engines, has been revived over the last decade. Flows arising in such devices lie at the intersection of compressible flows and chemically reacting flows. In addition, these flows are almost always turbulent. In order to first understand and then model the complicated physical mechanisms involved in high-speed reacting flows, one must therefore achieve a thorough understanding of the effects of compressibility and chemical reaction on turbulence.

In the field of compressible turbulence, research has been progressing at a remarkable pace in the past few years. Recent theoretical results are reviewed by Lele.[1] Extensive experimental work has been conducted, with a particular emphasis on supersonic plane mixing layers.[2–9] Explicit compressibility effects on the turbulence, such as the pressure dilatation correlation and the compressible (or dilatation) dissipation have been successfully modeled.[10–15] The limitations of existing incompressible models for terms such as the pressure–rate of strain correlation have been established,[16,17] and so has the need for future research, in both understanding and modeling the effects of compressibility on turbulence.

The body of literature concerning turbulent reacting flows is much more substantial. Reviews of the current status of both theoretical research and experimental work can be found in Refs. 18 and 19. The turbulent mixing layer has been the object of numerous experimental investigations, because this simple flow can be viewed as an elementary component of more complicated flows arising in combustion devices. Dimotakis[20] provides a thorough review of experimental and theoretical issues pertaining to this particular flow.

For flows involving combustion, probability density function (PDF) methods have demonstrated their ability to treat the important processes of reaction and convection exactly,[21] making transport and reaction models used in ordinary turbulence models unnecessary. This is believed to be an advantage over conventional Reynolds stress closures, which often resort to gradient-diffusion modeling for the triple correlation term in the Reynolds stresses evolution equation. For high Mach number flows, the dependence of the transport coefficients involved in these models on density is not known.[22] Furthermore, modeling the source term for reacting flows, which is necessary in a Reynolds stress closure approach, can be extremely difficult, at all Mach numbers.

Solving the modeled joint PDF transport equation using a Monte Carlo method involves using sets of stochastic particles with time-evolving properties to model fluid particles. The modeled transport equation for the joint PDF of velocity and composition has been successfully solved in this way.[23,24] Recent works include the development of models for the joint PDF of velocity and turbulent frequency,[25,26] and an extension of the range of applicability of PDF methods to flows with arbitrary pressure gradients.[27]

The application of PDF methods to compressible flows

is very recent.[28–31] The problem of determining the mean pressure directly from the stochastic particle properties is closely related to the difficulties encountered in trying to extend the PDF formulation to complex compressible flows. In the present work we follow up on previous research by the authors,[31] who proposed a new approach to extend PDF methods to high Mach number flows. One of the outstanding features of this approach is that it is entirely particle based: no coupling with a finite-volume algorithm to solve for variables such as the velocity or the pressure is necessary.

In this paper, the approach is extended further to account for chemical reaction with heat release. We take as our base flow the turbulent mixing layer, and the chemistry studied is the fast hydrogen–fluorine reaction. The pressure variations, which are neglected in low Mach number reaction modeling, are here fully taken into account. Source terms coming from viscous dissipation and pressure variations in the enthalpy equation are also represented. Even though finite reaction rates can be exactly accounted for using PDF methods, the nature of the reaction studied, for which the reaction time scale is much smaller than any of the relevant flow time scales, restricts the present approach to infinitely fast chemistry. The extension to finite rate chemistry is believed to be straightforward, but will not be addressed here.

In Sec. II, the simplifying assumptions for the chemistry are presented. In Sec. III we detail the PDF formulation, which is the object of this work, summarizing briefly the general idea behind PDF methods, then defining our stochastic variables and the corresponding stochastic differential equations (SDE). The fluid dynamics and turbulence aspects of the approach have been extensively addressed in Delarue and Pope,[31] hence the emphasis is here on the treatment of the reaction. In Sec. IV we present results for low Mach number mixing layers, which are compared with experimental data, and for high Mach number mixing layers. The results for the latter are compared to low Mach number results.

II. CHEMISTRY

The reaction we consider in this paper is the highly exothermic hydrogen–fluorine reaction:

$$H_2+F_2\rightarrow 2HF. \tag{1}$$

This reaction can be considered instantaneous, given the very high values of the reaction rate[32] and the time scales of interest in the turbulent mixing layer.[33] The reactants are not pure, but diluted in nitrogen N_2. Numerical values relevant to the description of the reactants, the dilutant and the reaction can be found in Table 1. The data in this table are reproduced from the JANAF tables.[34]

To describe the chemical composition at every point x and time t, we use the mixture fraction $\xi(x,t)$. In using the conserved scalar approach, we implicitly neglect the effects of differential diffusion in the flow. It has been shown[35] that these effects affect the shape of the PDF of mixture fraction, without, in general, affecting the mean values. In the following, we will concentrate on the mean temperature profiles, which are not affected by the difference in the species diffusivities. With the assumption that the reaction is infinitely fast and the knowledge of the instantaneous mixture fraction at every point in the domain, we can obtain in a simple way the mass fractions for all the species at the same location and time.[36] The relations between mass fractions and mixture fraction are shown in Fig. 1. The instantaneous species conservation equations can hence be replaced by the single instantaneous mixture fraction evolution equation.

TABLE I. Thermochemical properties of the relevant species.

	N_2	H_2	F_2	HF
W (g/mol)	28	2	38	20
ΔH_f^0(300 K)	0	0	0	−272.548
ΔH_f^0(700 K) (kJ/mol)	0	0	0	−273.522
c_p(300 K)	29.125	28.849	31.336	29.138
c_p(700 K) (J/K mol)	30.754	29.441	35.832	29.351
γ(300 K)	1.4	1.4	1.36	1.4
γ(700 K)	1.37	1.393	1.31	1.395

The calculations described in the following are based on the experimental investigations by Mungal and Dimotakis[33] and Hermanson and Dimotakis.[37] For these calculations, the reactants are modeled as ideal gases. The temperature rise in the experiments is never such as to necessitate taking into account the variations of the specific heats with temperature. Furthermore, in the temperature range of interest, it is safe to assume that the ratio of specific heats γ is identical for each species. The reader is referred to Table 1 for verification of the validity of these simplifying assumptions. We summarize them below:

$$c_{p,S}(T)=c_{p,S}, \quad \text{for each species S,} \tag{2}$$

$$\gamma_S=\gamma, \quad \text{for each species S.} \tag{3}$$

The error involved in making assumption (3) is smaller than the error involved in making assumption (2). The value we use for γ is $\gamma=1.38$. These assumptions allow for simpler equations in the PDF model presented in the next section.

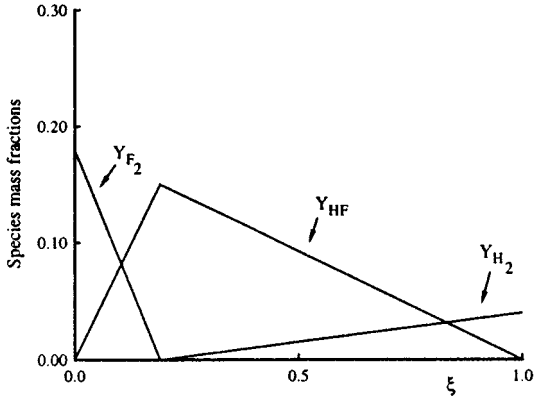

FIG. 1. Species mass fractions as a function of mixture fraction ξ. The stoichiometric mixture fraction is $\xi_s=0.19$. The mass fractions of reactants in the free streams are $Y_{F_2}=0.18$ and $Y_{H_2}=0.04$. The dilutant N_2 mass fraction is not shown.

The complete equations corresponding to the most general case, in which neither of these assumptions hold, are given in the Appendix.

For low-Mach number flows, two additional assumptions are generally made: the pressure is taken to be constant, and the specific enthalpy to behave as a conserved scalar.[38] The latter allows the instantaneous temperature to be simply related to the instantaneous mixture fraction, and the former, via the ideal gas equation of state, gives the instantaneous density as a function of the instantaneous mixture fraction. In low-Mach number flows, chemistry and fluid dynamics are coupled only through the dependence of the density on chemical composition.

In the case of low-Mach number turbulent flows, one cannot simply relate the mean temperature and density to the mean mixture fraction. To obtain the mean temperature and density at every point in the flow field, one needs to know the PDF $p(\xi)$ of the mixture fraction at that point. Some information on that PDF can be obtained if the mean and the variance of the mixture fraction are known. In a turbulent flow with high Reynolds number, the evolution equation for the mean (Favre-averaged) mixture fraction reads as

$$\langle\rho\rangle \frac{\partial\tilde{\xi}}{\partial t}+\langle\rho\rangle\tilde{U}_i \frac{\partial\tilde{\xi}}{\partial x_i}=-\frac{\partial\langle\rho\rangle\widetilde{u_i''\xi''}}{\partial x_i}. \tag{4}$$

In this equation the overtildes stand for Favre averages, the brackets for Reynolds averages, and the double primes for fluctuations about the Favre averages. The evolution equation for the variance of mixture fraction reads[36] as

$$\langle\rho\rangle \frac{\partial\widetilde{\xi''^2}}{\partial t}+\langle\rho\rangle\tilde{U}_i \frac{\partial\widetilde{\xi''^2}}{\partial x_i}=-2\langle\rho\rangle\widetilde{u_i''\xi_i''} \frac{\partial\tilde{\xi}}{\partial x_i}-\frac{\partial\langle\rho\rangle\widetilde{u_i''\xi''^2}}{\partial x_i} -2\langle\rho\rangle\mathscr{D}\frac{\partial\xi''}{\partial x_i}\,\partial\xi''\partial x_i. \tag{5}$$

In the above equation, $\mathscr{D}$ is the molecular diffusion coefficient, assumed to be uniform and identical for all species. The terms on the right-hand side of Eq. (5) represent, respectively, the production by the mean gradient, turbulent transport, and dissipation by molecular diffusion.

In high-Mach number flows, both pressure variations and enthalpy variations (other than those arising by simple mixing) have to be taken into account to determine the density or the temperature in the flow field. The species mass fractions, however, remain functions of the mixture fraction alone, since the basic assumption underlying the mixture fraction approach—namely, that the reaction rates are infinitely fast when compared to the flow time scales—still holds for the range of Mach numbers (roughly between 0 and 6.5) considered here. However, the knowledge of the PDF of the mixture fraction becomes insufficient to determine the mean temperature and mean density at any point in the flow field. One needs to know also the PDF of two independent thermodynamic variables, pressure, and enthalpy, for example. In the model we present in the next section, we address these issues, and allow the additional coupling between fluid dynamics and chemistry arising from pressure and enthalpy variations to be accurately represented.

III. DESCRIPTION OF THE PDF MODEL

Part of what follows has been treated in more detail in Delarue and Pope.[31] We will therefore cover only the aspects of the presentation that are new or essential to a good understanding of the paper.

A. The Eulerian mass density function

In a turbulent compressible reacting flow, it is common to consider the flow properties U, ω (turbulent frequency), ξ, e (specific internal energy), and p (pressure) at any fixed location x and time t as random variables. If we denote the sample space variables associated with these random flow variables with an overcaret ($\hat{}$), we define the one-point Eulerian mass-density function $\mathscr{F}$ as

$$\mathscr{F}(\hat{U},\hat{\omega},\hat{\xi},\hat{e},\hat{p};x,t)=\rho_s(\hat{e},\hat{p},\hat{\xi})\langle\delta(U(x,t)-\hat{U}) \times\delta[\omega(x,t)-\hat{\omega}]\delta[\xi(x,t)-\xi] \times\delta[e(x,t)-\hat{e}]\delta[p(x,t)-\hat{p}]\rangle. \tag{6}$$

In this definition δ is the Dirac delta function, and p_s is the equation of state giving the fluid density as a function of specific internal energy, pressure, and mixture fraction. We can obtain the fluid density at any point and time by

$$\rho(x,t)=\rho_s[e(x,t),p(x,t),\xi(x,t)].$$

The knowledge of $\mathscr{F}$ enables one to compute statistics of the flow, simply by computing its moments. One can derive an evolution equation for $\mathscr{F}$ from the Navier–Stokes equations, but it contains unclosed terms, which need to be modeled. In the following section we briefly address this issue.

B. Particle representation

In a Monte Carlo simulation of a flow with total mass M, $\mathscr{F}$ is represented by an ensemble of N stochastic particles, each of mass $\Delta m=M/N$, which model fluid particles. In our representation, each stochastic particle i has a position $x^{(i)}$, a velocity $U^{(i)}$, a turbulent frequency $\omega^{(i)}$, a mixture fraction $\xi^{(i)}$, a pressure $p^{(i)}$, and a specific internal energy $e^{(i)}$. All these properties depend only on time t, and evolve according to modeled evolution equations. The discrete Lagrangian mass–density function is defined as

$$\mathscr{F}_N(\hat{U},\hat{\omega},\hat{\xi},\hat{e},\hat{p},x;t)=\Delta m\sum_{i=1}^{N}\delta(U^{(i)}-\hat{U}) \times\delta(\omega^{(i)}-\hat{\omega})\,\delta(\xi^{(i)}-\hat{\xi})\,\delta(e^{(i)}-\hat{e}) \times\delta(p^{(i)}-\hat{p})\,\delta(x^{(i)}-x). \tag{7}$$

The modeled evolution equations for the stochastic particle properties yield an evolution equation for $\mathscr{F}_N$, which constitutes our model for the evolution equation for $\mathscr{F}$. The moments of $\mathscr{F}_N$ give the statistics of particle properties, which we require to model the corresponding statistics of the flow.

C. Modeled particle evolution equations

The modeled evolution equations for the particle properties are written as stochastic differential equations (SDE) in which $d\alpha^* = d\alpha^*(t)$ denotes the infinitesimal increment $\alpha^*(t+dt) - \alpha^*(t)$ for any stochastic particle property α^*.

The formulation has been designed for the most general case, with finite rate chemistry and variable specific heats. In the following, we only detail the equations relevant to reacting flows in which simplifications (2) and (3) hold. The reader is referred to the appendix for the general equations.

The particle position, velocity, and turbulent frequency evolve according to the same evolution equations as have been detailed in Delarue and Pope.[31] We restate them briefly below:

$$dx^* = U^*\, dt, \tag{8}$$

$$dU_i^* = -\frac{1}{\langle\rho\rangle}\frac{\partial\langle p\rangle}{\partial x_i}\, dt + \frac{1}{2k}\left[\frac{\Pi_d}{\langle\rho\rangle} - \epsilon\left(1+\frac{3}{2}C_0\right)\right] \times (U_i^* - \widetilde{U}_i)dt + (C_0\epsilon)^{1/2}\, dW_i, \tag{9}$$

$$d\omega^* = -(\omega^* - \widetilde{\omega})C_3\Omega - \widetilde{\omega}\omega^* S_\omega\, dt + (2\sigma^2\widetilde{\omega}\omega^* C_3\Omega)^{1/2}\, dW. \tag{10}$$

In the above system, the terms in dW and dW_i are one- and three-dimensional independent Wiener processes, or Brownian motion increments. Equation (8) merely states that each stochastic particle moves with its own velocity. Equation (9) is the simplified Langevin model[39] for the velocity modified to account for the effects of compressibility on turbulence, and Eq. (10) is the Jayesh and Pope[40] model for the turbulent frequency. In the above equations, Π_d is the pressure–dilatation correlation $\langle p' u'_{i,i}\rangle$, and ϵ is the dissipation rate of turbulent kinetic energy, which incorporates the compressible dissipation $4/3\nu\langle u'^2_{i,i}\rangle$. The models for the effects of compressibility on turbulence incorporated in these equations are Zeman's pressure–dilatation model[14] and the Sarkar *et al.* model for the compressible dissipation.[10] No attempt has been made to account for the effects of compressibility on the pressure–rate of strain correlation. Also, the dependence of the fluctuating dilatation rate $u'_{i,i}$ on chemical composition fluctuations has not been considered: the models for the pressure–dilatation correlation and for the compressible dissipation take into account the density variations arising from pressure variations alone.

The particle mixture fraction ξ^* changes because of molecular mixing alone—the mixture fraction is a conserved scalar. The mixing model used in this paper is the IEM model proposed by Dopazo.[41] Hence the evolution equation for ξ^*:

$$d\xi^* = -C_\phi\Omega(\xi^* - \widetilde{\xi})dt. \tag{11}$$

In the above equation, C_ϕ is a model constant equal to 1, and Ω is related to the mean turbulent frequency.

The particle specific internal energy is decomposed into chemical energy and sensible energy:

$$e^* = e_c^* + e_s^*,$$

with, if the mixture consists of n species,

$$e_c^* = \sum_{i=1}^{n} Y_i^*\, \Delta H_{f,i}^0,$$

$$e_s^* = \sum_{i=1}^{n} Y_i^* c_{v,i} T.$$

In the above system, Y_i^* is the particle mass fraction of species i, known if the particle mixture fraction ξ^* is known, and $\Delta H_{f,i}^0$ is the specific enthalpy of formation for species i. We take the reference temperature to be 0 K. We have used our assumption of constant specific heats.

The evolution equation for the particle specific internal energy is derived from the first law of thermodynamics:

$$de^* = \epsilon\, dt - C_\phi\Omega(h^* - \widetilde{h})dt - p^*\, dv^*. \tag{12}$$

In the above equation, v^* refers to the specific volume of the stochastic particle, related to e^*, p^*, and ξ^* by the equation of state, which, for a mixture of n ideal gases with constant specific heats and identical ratio of specific heats [cf. assumptions (2) and (3)] reads as

$$p^* v^* = (\gamma-1)e_s^*, \quad = (\gamma-1)\left(e^* - \sum_{i=1}^{n} Y_i^*\, \Delta H_{f,i}^0\right). \tag{13}$$

In our case, the enthalpies of formation for all but one of the species, HF, are zero, and the equation of state simplifies to

$$p^* v^* = (\gamma-1)(e^* - Y_{\mathrm{HF}}^*\, \Delta H_{f,\mathrm{HF}}^0). \tag{14}$$

The above equation enables us to compute dv^* if de^*, dp^*, and dY_i^* (or $d\xi^*$) are known.

The term corresponding to heat addition in Eq. (12) contains two contributions: the first one, the first term on the right-handside, corresponds to viscous dissipation, and the second one, the second term on the right-hand side, to molecular heat fluxes. The latter involves the particle specific enthalpy, $h^* = e^* + p^* v^*$, and the mean enthalpy $\widetilde{h}$. We neglected all heat losses due to radiation, which is legitimate provided the temperature rise is not too large. We will see that such is the case here.

If the energy variable is taken to be the specific enthalpy, the stochastic differential equation equivalent to (12) is

$$dh^* = \epsilon\, dt - C_\phi\Omega(h^* - \widetilde{h})dt + v^*\, dp^*. \tag{15}$$

In the low-Mach number limit, the viscous dissipation and the pressure variations can be neglected (see the scaling analysis further on), and Eq. (15) reduces to the evolution equation for the mixture fraction, Eq. (11), which is consistent with the approximation that the enthalpy behaves as a conserved scalar in this limit. For reasons given in Delarue and Pope,[31] we choose the specific internal energy as our energy variable.

The pressure equation is fully modeled. We write it in a general form:

$$dp^* = p^*(A\, dt + B\, dW). \tag{16}$$

The two model coefficients A and B are given by

$$A=\frac{\epsilon}{e_s^*}-\frac{C_\phi}{e_s^*}\,\Omega(h^*-\widetilde{h})+\frac{B^2}{2}\left(1+\frac{1}{\gamma}\right)-\gamma\left(\frac{\partial\langle U_i\rangle}{\partial x_i}-\Omega_A(p^*-\langle p\rangle)\right)-\sum_{i=1}^{n}\frac{dY_i^*}{dt}\,\frac{\Delta H_{f,i}^0}{e_s^*},\qquad(17)$$

$$B^2=\frac{p_e^2}{\tau_a}\,\frac{1}{\theta}\,\frac{1}{(\langle\rho\rangle\widetilde{a})^2}\,\frac{1}{\widetilde{e}-\Sigma_{i=1}^{n}\widetilde{Y}_i\,\Delta H_{f,i}^0}.\qquad(18)$$

In the above equations, p_e and τ_a are given by Zeman,[14] $\theta=1-\gamma^{-1}$, and $\widetilde{a}=\gamma\langle p\rangle/\langle\rho\rangle$ is the mean local speed of sound. Here Ω_A is given in the appendix. The rate of formation dY_i^*/dt appears in Eq. (17): it can be easily calculated given the rate of change of mixture fraction, Eq. (11), and the correspondence between Y_i^* and ξ shown in Fig. 1.

More details on the conditions that lead to the exact determination of the model coefficients A and B can be found in Delarue and Pope.[31] Briefly, it can be stated that the first term on the left-hand side of Eq. (17) corresponds to heat added by viscous dissipation, the second term corresponds to heat added by turbulent mixing of enthalpy [and as such has the same form as the corresponding term in the particle enthalpy equation, Eq. (15)], the following two terms correspond to the total pressure–dilatation correlation (the mean part being in closed form, and the turbulent part being modeled according to Zeman's model), and the last term corresponds to heat added by the chemical reaction. It is seen that Lagrangian pressure varies mainly because of heat release and dilatation work. The expression for B, Eq. (18), allows a constant level of pressure variance of approximately p_e^2 to be maintained in flows for which the acoustic time scale τ_a is much smaller than the turbulent time scale k/ϵ. This model level of turbulent pressure fluctuations has been introduced by Zeman,[14] based on findings by Sarkar *et al.*[10,42]

It should be noted that the model equation for pressure, Eq. (16), is not restricted to small departures from a constant state. Flows in which the pressure field exhibits large spatial variations can be dealt with. However, shocks and discontinuities, though theoretically tractable, are, in practice, very difficult to address. The reasons for this will be given in the last section.

In the present case, where HF is the only species for which the enthalpy of formation is not zero, we rewrite Eqs. (17) and (18) as

$$A=\frac{\epsilon}{e_s^*}-\frac{C_\phi}{e_s^*}\,\Omega(h^*-\widetilde{h})+\frac{B^2}{2}\left(1+\frac{1}{\gamma}\right)-\gamma\left(\frac{\partial\langle U_i\rangle}{\partial x_i}-\Omega_A(p^*-\langle p\rangle)\right)-\frac{dY_{\rm HF}^*}{dt}\,\frac{\Delta H_{f,\rm HF}^0}{e_s^*},\qquad(19)$$

$$B^2=\frac{p_e^2}{\tau_a}\,\frac{1}{\theta}\,\frac{1}{(\langle\rho\rangle\widetilde{a})^2}\,\frac{1}{\widetilde{e}-\widetilde{Y}_{\rm HF}\,\Delta H_{f,\rm HF}^0}.\qquad(20)$$

The determination of the mean pressure field directly from the particle properties is a simple matter with the presented formulation: one just needs to average the particle pressure p^* over the ensemble of particles. An alternate approach, in which the resulting pressure field can be smoothed and filtered, is presented in Delarue and Pope.[31]

Once the particle energy, pressure, and mixture fraction are known, it is a simple matter to obtain the particle temperature, using the ideal gas equation of state:

$$T^*=\frac{p^*v^*}{R\sum_{i=1}^{n}\frac{Y_i^*}{W_i}}.\qquad(21)$$

In this equation R is the universal gas constant and W_i is the molar weight of species i. We have shown[31] that for any particle property, both the Favre average and the Reynolds average could be obtained from the model joint PDF $\mathscr{F}_N$. Equation (21) therefore allows us to output the Reynolds-averaged temperature at any point in the flow domain, for comparison with experimental data.

The modeled particle evolution equations, Eqs. (8), (9), (10), (11), (12), and (16) yield an evolution equation for the model joint PDF, $\mathscr{F}_N$, with no unclosed terms. The evolution equations for the moments of $\mathscr{F}_N$ constitute model equations for the corresponding moments of $\mathscr{F}$. For instance, the mean and the variance of mixture fraction evolve according to

$$\langle\rho\rangle\,\frac{\partial\widetilde{\xi}}{\partial t}+\langle\rho\rangle\widetilde{U}_i\,\frac{\partial\widetilde{\xi}}{\partial x_i}=-\frac{\partial\langle\rho\rangle\widetilde{u_i''\xi''}}{\partial x_i},\qquad(22)$$

$$\langle\rho\rangle\,\frac{\partial\widetilde{\xi''^2}}{\partial t}+\langle\rho\rangle\widetilde{U}_i\,\frac{\partial\widetilde{\xi''^2}}{\partial x_i}=-2\langle\rho\rangle\widetilde{u_i''\xi_i''}\,\frac{\partial\widetilde{\xi}}{\partial x_i}-\frac{\partial\langle\rho\rangle\widetilde{u_i''\xi''^2}}{\partial x_i}-2\langle\rho\rangle C_\phi\Omega\widetilde{\xi''^2}.\qquad(23)$$

Comparing Eqs. (4) and (22) on the one hand, and Eqs. (5) and (23) on the other hand, one sees that the only modeled term in the particle moments evolution equations is the dissipation by molecular diffusion. The remaining terms are all in closed form. This is a consequence of convection being treated exactly in the Lagrangian PDF formulation.

The modeled evolution equation for the mean enthalpy reads as

$$\langle\rho\rangle\,\frac{\partial\widetilde{h}}{\partial t}+\langle\rho\rangle\widetilde{U}_i\,\frac{\partial\widetilde{h}}{\partial x_i}=\langle\rho\rangle\langle\epsilon\rangle+\left\langle\frac{Dp}{Dt}\right\rangle-\frac{\partial\langle\rho\rangle\widetilde{u_i''h''}}{\partial x_i}.\qquad(24)$$

In the above equation, Dp/Dt is the subtantial derivative of the pressure, which appears in closed form with our model.

We will now try to obtain the low-Mach number limit for this equation. In a mixing layer for which the velocity difference between the fast stream and the slow stream is ΔU, and the width of the turbulent region at downstream location x is $\delta(x)$, the turbulent dissipation ϵ scales like $\Delta U^3/\delta(x)$.[43] Furthermore, we can estimate the mean pressure decrease in the center of the layer to be $\langle\rho\rangle\widetilde{v''^2}$, which we can approximately scale like $\langle\rho\rangle\Delta U^2$.[43] The time scale at which the Lagrangian mean pressure varies inside the turbulent region can be estimated to be roughly $\delta(x)/\Delta U$—this means that the mean pressure following a fluid particle will vary only if the fluid particle cross-stream position changes.

Hence, in Eq. (24), the viscous dissipation term and the substantial derivative of the pressure both scale like $\langle\rho\rangle\Delta U^3/\delta(x)$ (provided the turbulent pressure fluctuations are small compared to the mean pressure, which is usually the case). The turbulent enthalpy flux can be taken to scale like $\langle\rho\rangle c_p\ \Delta U\ \Delta T/\delta(x)$, where ΔT is the temperature difference between the two streams and c_p is the specific heat at constant pressure for the mixture inside the turbulent region (we assume, for the sake of scaling, that turbulent enthalpy and turbulent velocity fluctuations are perfectly correlated). Compared to the other two terms, the turbulent enthalpy flux therefore scales like $c_p\ \Delta T/\Delta U^2$. If T_0 is some reference temperature, and c_0 the corresponding speed of sound for an ideal gas (we can choose these values from one of the free streams), then the scaling can be rewritten as $1/M_c^2\ \Delta T/T_0$, where M_c is the Mach number based on the velocity difference and the reference speed of sound. In this scaling we neglected the influence of the coefficient of correlation between turbulent enthalpy and turbulent velocity fluctuations, as well as a factor containing the ratio of specific heats. Both factors are of order unity, and we neglected them to obtain a simpler expression. The scaling thus shows that for low-Mach number, the turbulent enthalpy flux dominates the other terms. This fact is consistent with the model behavior of the enthalpy as a conserved scalar in this limit [see Eq. (15)]: the only important effect is passive mixing arising from temperature differences between the two streams. The low-Mach number form of Eq. (24), obtained therefore simply by neglecting the pressure variations and the viscous dissipation, is the same as Eq. (4). For the other modeled moments evolution equations, the reader is referred to Delarue and Pope.[31]

IV. IMPLEMENTATION IN SUBSONIC AND SUPERSONIC SHEAR LAYERS

A. Dimensional analysis

Consider a reacting mixing layer, for which both streams are mixtures of ideal gases, with assumptions (2) and (3) holding. The dimensional parameters needed to fully describe the flow, in the high Reynolds and Péclet numbers limit, are the pressures p_i, the densities ρ_i, the velocities U_i, and for each species j, the mass fraction $Y_{i,j}$ of that species in the ith free stream, the molar weight W_j, the specific enthalpy of formation $\Delta H^0_{f,j}$ and the ratio of specific heats γ_j.

The corresponding nondimensional parameters are

$$\frac{p_2}{p_1},\frac{\rho_2}{\rho_1},\frac{U_2}{U_1},M_1,Y_{i,j},\frac{W_j}{W_1}\ (j=2,...,n),\gamma_j,\frac{\Delta H^0_{f,j}\ \rho_1}{p_1}. \tag{25}$$

In the above set, M_1 is the free-stream Mach number in the first stream (which is taken to be the high-speed stream). The experiments on which the following calculations are based have a pressure ratio p_2/p_1 of 1, a density ratio ρ_2/ρ_1 of 1, and a velocity ratio U_2/U_1 of 0.4. The molar weights for each species are given in Table 1, and the γ_j's have all been taken to be 1.38. The mass fractions in the free streams are different for each run. These are low-Mach number experiments, for which M_1 is found to be approximately 0.17. Finally, the parameter $\Delta H^0_{f,\mathrm{HF}}\ \rho_1/p_1$, which in the following we will denote by K, is approximately 153.

The fact that the pressures, the densities, and the ratios of specific heats are identical in each free stream allows us[31] to replace M_1 by a more meaningful parameter, the convective Mach number:[3,44]

$$M_c=\frac{U_1-U_2}{2c}=\frac{\Delta U}{2c} \tag{26}$$

to describe the level of compressibility of the flow. In Eq. (26), c is the common value of the speed of sound in each free stream.

For our particular chemistry, we can rewrite Eq. (1) in terms of mass and not of number of moles, as

$$\mathrm{H_2}+r\mathrm{F_2}\rightarrow(1+r)\mathrm{HF}.$$

This merely states that one unit of mass of H_2 reacts with r units of mass of F_2 to form $(1+r)$ units of mass of HF. The value of r is 19. If, in our reacting mixing layer, the mass fractions of H_2 and F_2 in the free streams are $Y_{\mathrm{H_2}}$ and $Y_{\mathrm{F_2}}$, respectively (there is only one reactant per free stream), the maximum mass fraction of HF that can be formed inside the layer is[36]

$$Y_{\mathrm{HF,max}}=\frac{(1+r)Y_{\mathrm{H_2}}Y_{\mathrm{F_2}}}{rY_{\mathrm{H_2}}+Y_{\mathrm{F_2}}}. \tag{27}$$

Hence the quantity $Y_{\mathrm{HF,max}}\ \Delta H^0_{f,\mathrm{HF}}$ represents the maximum change in sensible energy (which is roughly proportional to the maximum change in temperature) brought about, within the mixing region, by the chemical reaction.

From the above analysis, we can predict what the high-Mach number behavior of the flow will be, compared to the low-Mach number behavior. Consider a flow in which all the parameters listed in (25) are held constant, except the convective Mach number M_c, which continually increases. Consider the parameter K_T, defined as

$$K_T=Y_{\mathrm{HF,max}}K,$$

with $Y_{\mathrm{HF,max}}$ given by (27). Here, K_T is also held constant, and we can rewrite it as

$$K_T=Y_{\mathrm{HF,max}}\frac{\Delta H^0_{f,\mathrm{HF}}\ \rho_1}{p_1}=Y_{\mathrm{HF,max}}\frac{\Delta H^0_{f,\mathrm{HF}}\ \gamma}{c^2},$$

where $\gamma=1.38$ is the common value of the ratio of specific heats for all species. Making use of the definition of M_c as $\Delta U/2c$, we can further modify our expression to obtain

$$\frac{Y_{\mathrm{HF,max}}\ \Delta H^0_{f,\mathrm{HF}}}{\Delta U^2}=\frac{K_T}{4\gamma M_c^2}. \tag{28}$$

With the assumption that all parameters, including K_T, are held constant but for M_c that increases, Eq. (28) tells us that the parameter $Y_{\mathrm{HF,max}}\ \Delta H^0_{f,\mathrm{HF}}/\Delta U^2$, which represents the ratio of the temperature rise coming from chemical heat release to that coming from fluid dynamical effects, goes to zero as the Mach number goes to infinity. For high Mach number flows, therefore, we expect the temperature rise coming from

TABLE II. Molar and mass fractions for different runs.

ϕ	c_{F_2}	Y_{F_2}	c_{H_2}	Y_{H_2}	ξ_s	ΔT_f (K)
1	0.01	0.014	0.01	0.0007	0.5	93
1	0.03	0.04	0.03	0.002	0.5	278.1
1	0.05	0.067	0.05	0.0037	0.5	456.8
4,1/4	0.01	0.014	0.04	0.003	0.19	149
8,1/8	0.01	0.014	0.08	0.006	0.1	165

heat release to become insignificant, compared to that coming from effects such as the viscous dissipation. The behavior of high-Mach number reacting flows, in other words, should be a little different from that of high-Mach number inert flows.

B. Low-Mach number calculations

All the calculations presented in this section have been made with a value of 0.17 for M_1, which corresponds to a value of 0.07 for M_2, and of 0.052 for M_c. The particle properties are advanced in time using the model equations described above. A typical simulation used approximately 500 000 particles on a 18×58 grid, a number large enough to obtain smooth second and third moments of the flow fields, but too small to guarantee a sufficiently stable pressure field. Therefore, the mean pressure was determined using the algorithm described in Delarue and Pope,[31] which amounts to solving an elliptic equation in the low-Mach-number limit. The calculations were initialized with given profiles for the first-order moments and the Reynolds stresses. The splitter-plate tip is not represented in the computational domain: therefore, all subsequent plots involving the virtual origin x_0 assume that this point lies at the intersection of the two straight lines enclosing the turbulent region in the self-similar regime.

The first series of calculations corresponds to low values of the heat release, after the ''flip'' experiments of Mungal and Dimotakis.[33] In our calculations, the molar fraction of F_2 in the high-speed stream is kept constant, at 1%, while the molar fraction of H_2 takes on the values 1%, 4%, and 8%. The corresponding mass fractions Y_{H_2} and Y_{F_2}, and values of the stoichiometric mixture fraction ξ_s, given by[36]

$$\xi_s = \frac{Y_{F_2}}{Y_{F_2} + r Y_{H_2}}$$

are given in Table II, as well as the adiabatic flame temperatures ΔT_f for each case. Therefore, the mixture starts from stoichiometric proportions, and the reactant on the low-speed side becomes increasingly richer. The reactants are then ''flipped:'' the molar concentrations in each free stream remain unchanged, but the fluorine is moved to the low-speed stream, and the hydrogen to the high-speed stream. A useful quantity to characterize each flow is the equivalence ratio ϕ:[33]

$$\phi = \frac{c_{02}/c_{01}}{(c_{02}/c_{01})_s} = \frac{c_{02}}{c_{01}}, \tag{29}$$

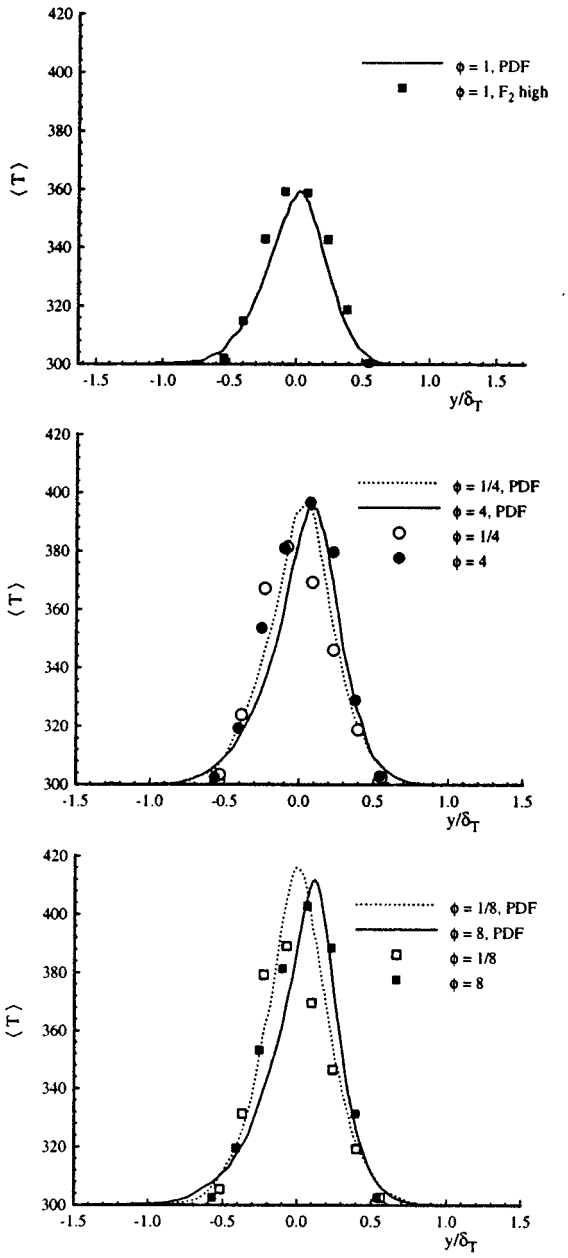

FIG. 2. Mean temperature rise, low heat release: top, ϕ=1°; middle: ϕ=4, 1/4°; bottom: ϕ=8, 1/8. Lines: calculations. Symbols: experiments (Ref. 33).

where c_{02} and c_{01} are the low-speed and high-speed reactant molar concentrations, and $(c_{02}/c_{01})_s$ is the ratio of these concentrations when the reactants are in stoichiometric proportions. The simplification in Eq. (29) comes from the fact [cf. Eq. (1)] that $(c_{02}/c_{01})_s = 1$. Thus, for flows with a lean low-speed stream reactant, $\phi \leqslant 1$, and $\phi \geqslant 1$ for flows with a rich low-speed stream reactant.

The results for these runs are presented in Fig. 2. All the temperature profiles in this section are plotted versus y/δ_T, where δ_T is the 10% thickness of the temperature profile.

The agreement is overall quite good for equivalence ratios ϕ greater than 1. The model predicts the skewing of the profiles toward the lean reactant, F_2, and the locations and values of the peak temperature rise are well reproduced. The

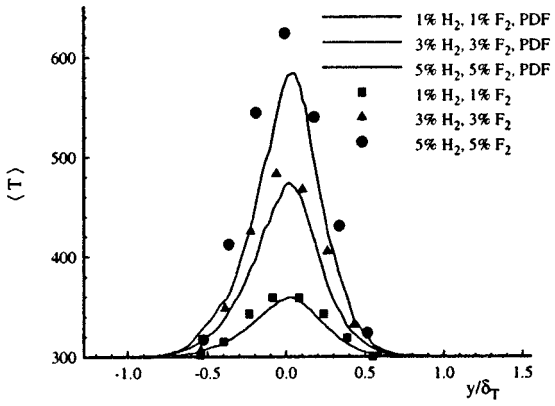

FIG. 3. Mean temperature rise, high heat release. Solid lines: calculations. Symbols: experimental data (Ref. 37).

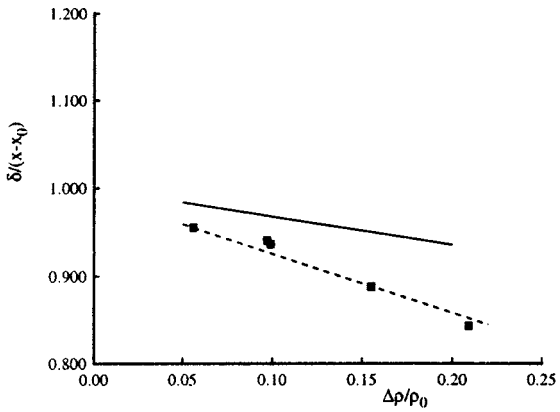

FIG. 4. Decrease of the layer growth rate with increasing heat release. Solid line: best fit to the experimental data (Ref. 37). Dashed line: best fit to the calculations. Some sample calculations are shown (symbols).

temperature profile is not as full in the center region as the experimental profiles, resulting in an overall smaller total amount of product formed (which, in the low-Mach number case, is proportional to the temperature rise). In this fast chemistry limit, the amount of product formed is mixing limited. The underprediction of the amount of product formed is therefore traceable to the mixing model: in our calculations, the fluid is not mixed well enough.

For the runs with an equivalence ratio smaller than 1, in which case the high-speed stream reactant is rich, the skewing of the profiles toward the lean reactant is also well reproduced, as well as the location of the peak temperature rise. However, the experimental data exhibit an overall decrease of the peak temperature rise, which has been attributed to an asymmetry in the entrainment,[33] resulting in values greater than one for the entrainment ratio, which is the ratio of the volume of high-speed fluid entrained to that of low-speed fluid entrained. Our calculations do not reproduce that effect: the peak temperature rise is the same as in the case where the low-speed stream reactant is rich, and the entrainment ratio is close to one for all our runs. The source of the problem has been traced to the turbulent frequency model, which predicts a symmetric entrainment on both sides of the layer. The pressure and energy equations, which are the centerpiece of this work, are not at fault. Improvement is, however, needed in modeling the evolution of the particle turbulent frequency.

For the second series of calculations, the heat release is increased, and its effect on the layer growth rate is studied. The reactants are in stoichiometric proportions, but their molar concentrations are increased until they teach 5% in each stream. The corresponding mass fractions are given in Table II, as well as the adiabatic flame temperatures.

Figure 3 shows the mean temperature rise for three cases. Again, the calculations compare well with the experimental results, but the amount of product is underpredicted. Hermanson and Dimotakis[37] find that the layer growth rate decreases with increasing heat release. Figure 4 shows the decrease in the layer growth rate resulting from increasing heat release in our calculations. To remove the dependence upon the particular thickness used in measuring the growth rate, the data have been normalized by the extrapolated value of the straight lines at zero heat release. The parameter against which the growth rate is plotted is

$$\frac{\Delta\rho}{\rho_0} = 1 - \int_{\eta_1}^{\eta_2} \frac{T_0}{T_0 + \langle \Delta T \rangle)}\, d\eta,$$

where η_1 and η_2 are the 1% points of the mean temperature profile, and η is the corresponding similarity coordinate. Here T_0 and ρ_0 are the free-stream values of the temperature and density, identical for each free stream. The slope of the best fit to the calculations is reasonably close to that of the best fit to the experimental data, albeit a little steeper. It should be noted that, because of the underprediction of product formation mentioned above, the highest value of $\Delta\rho/\rho_0$ reached in the calculations is 0.21, versus 0.28 for the same case (5% of reactant in each stream) in the experiments.

The calculated values of the spreading rate for δ_T were on average larger than the experimental values: for the run in which the free-stream molar concentrations are set to 1%, the layer grows about 45% faster in our calculations than in the experiments. This can be attributed to three causes: the first one is the inaccuracy in the exact determination of the 10% thickness from both the experimental plots (the experimental results reporting numerically only the 1% thickness, very difficult to use in our case) and our calculations. If there is a 10% error in the width of the turbulent region as given by δ_T, there will be a 10% error in the layer growth rate as well. The second cause lies in the extreme simplicity of the temperature mixing model used, namely the IEM model. It is known to occasionally allow very hot particles to leave the center of the turbulent region without reducing their temperatures quickly enough. This might account for the temperature mixing layer being somewhat too wide in the self-similar regime. Finally, the third cause lies in an overprediction of the Reynolds shear stress $\langle \rho u' v' \rangle$ in the center of the layer, as is evident in Fig. 5. This overprediction is an effect of the simplified Langevin model used in the velocity equation, and yields and excessive production of turbulent kinetic energy.

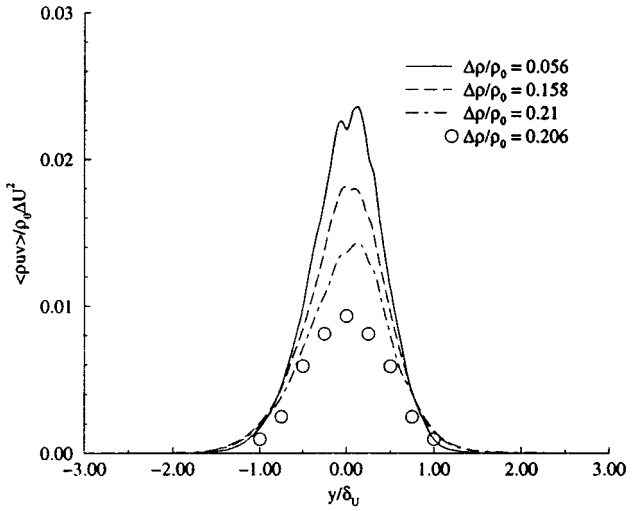

FIG. 5. Effect of increasing heat release on Reynolds shear stress. Lines: PDF results. Symbols: experimental data (Ref. 37).

However large the calculated growth rate may be, it still lies in the acceptable range of growth rates.[45] As the heat release increases, the gap between calculated growth rates and experimental ones is slightly reduced, as can be seen from Fig. 4: the calculated spreading rates decrease somewhat faster than the experimental ones.

The decrease of the growth rate has been traced[37] to a decrease in the Reynolds shear stress. Figure. 5 shows that this is also the case in the calculations. The similarity coordinate is here y/δ_U, where δ_U is the 10% thickness of the mean velocity profile. As in the experiments, the decrease in the shear stress comes exclusively from the density decrease due to heat release. The broadening of the profiles, noted in the experiments, is evident on the plot. The experimental data plotted in Fig. 5 clearly show that for the same amount of product formed, as measured by $\Delta\rho/\rho_0$, the calculation overpredicts the Reynolds shear stress peak.

Finally, it should be emphasized that there is no theoretical restriction on the amount of heat release in the formulation of the model equations. The only issues to consider when dealing with flows involving very high local temperature rises are numerical ones: if there is a very important temperature gradient locally, it becomes necessary to refine the grid and increase the number of stochastic particles. However, if discontinuities appear as in highly compressible flows, the amount of particles and of grid refinement necessary to resolve them become prohibitive. This point is discussed further in the next section.

C. High-Mach number calculations

The purpose of these low-Mach number calculations was to gain an appreciation for the overall performance of the models in the cases reported above. These calculations were rendered necessary by the lack of experimental data on supersonic reacting shear layers. Having established the close match between our PDF calculations and the experimental data at low Mach number, at least for flows with $\phi \geqslant 1$, we therefore proceed to study the same cases at a higher value of the free-stream Mach number M_1.

In the following calculations, the cases corresponding to low heat release and a value of the equivalence ratio greater than one (1% F_2 in the high-speed stream, 1%, 4%, and 8% H_2 in the low-speed stream) are studied at a value of the Mach number M_1 of 2.69. The low-speed Mach number for these cases is $M_2 = 1.08$, and the convective Mach number is $M_c = 0.81$.

The models we are using for the effects of compressibility on turbulence will have the following effects: Zeman's model for the pressure–dilatation will ensure that the level of turbulent pressure fluctuations relaxes to the equilibrium value p_e, roughly equal to $M_t^2\langle p\rangle$, on the acoustic time scale τ_a, which is small compared to the turbulent time scale—the ratio between these two time scales being the turbulent Mach number, which never exceeds 0.4 in our calculations. This means that the magnitude of the pressure–dilatation, proportional to the gap between p_e^2 and $\langle p'^2\rangle$, will be small. Its effect on the mean pressure, mean internal energy, and turbulent kinetic energy will thus be small. The dominant effect of compressibility on turbulence will therefore be the compressible dissipation. Recent evidence shows that this is not the case,[46] but the lack of better models makes the dominant physical effects of compressibility on turbulence—which consist of a decrease in the redistribution of energy between the components of the Reynolds stress tensor—extremely hard to reproduce. For the time being, we therefore stick to Sarkar's model, which will predict an increased dissipation of turbulent kinetic energy, and subsequently an isotropic decrease in the magnitude of the diagonal Reynolds stresses. We also expect this increased dissipation to increase the temperature peak in the center of the turbulent region, since we have seen that dissipation becomes an increasingly important contributor to overall heat release as the Mach number increases.

The following results focus on mean temperature profiles. Instead of plotting these versus a particular similarity coordinate, we plot them at a given downstream location x, versus the nondimensional coordinate $y/(x-x_0)$, where x_0 is the location of the virtual origin. We intend to show in this way that the profiles become narrower when the compressibility increases. The downstream distance x is chosen so as to match the downstream distance at which the self-similar profiles were computed in the previous section, which is shortly after the onset of self-similarity for the Reynolds stress profiles.

Figure 6 shows the results for the high Mach number case, compared to the low Mach number results of the previous section. We confined ourselves to flows with $\phi \geqslant 1$, for which we have shown the close correspondence between experimental data and our PDF calculations. Two trends are apparent: (i) the layer is narrower, at the same downstream location, in the high-Mach number case than in the low-Mach number case; and (ii) the peak value of the temperature profile is higher at higher Mach number. These results are not surprising. The decreased width of the layer comes from the well-known fact that the spreading rate of a mixing layer

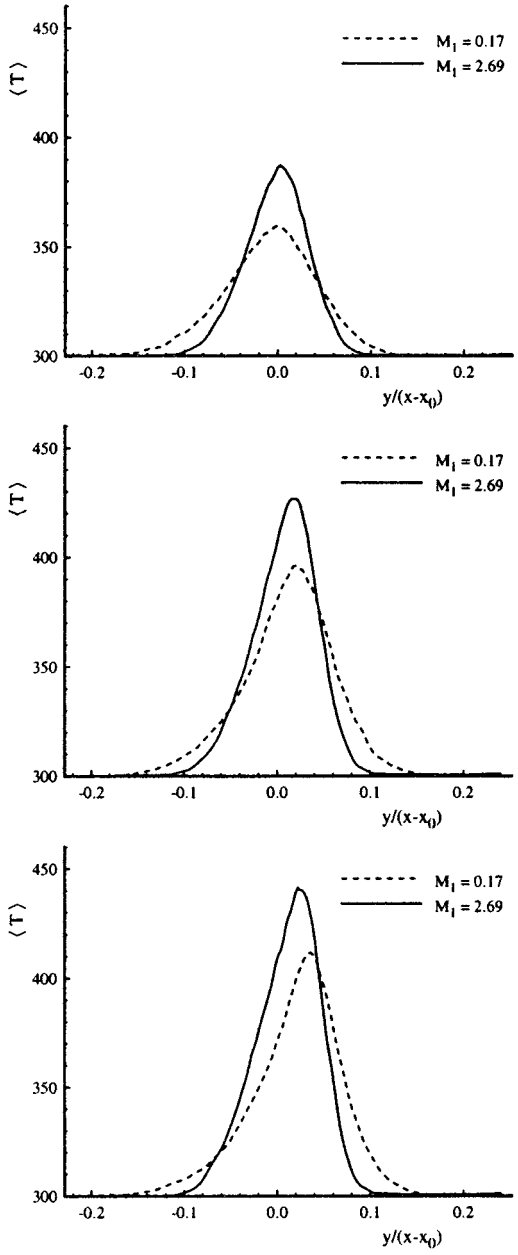

FIG. 6. Effect of increasing Mach number on the mean temperature profiles at the same downstream location. Top: $\phi=1$; middle: $\phi=4$; bottom: $\phi=8$.

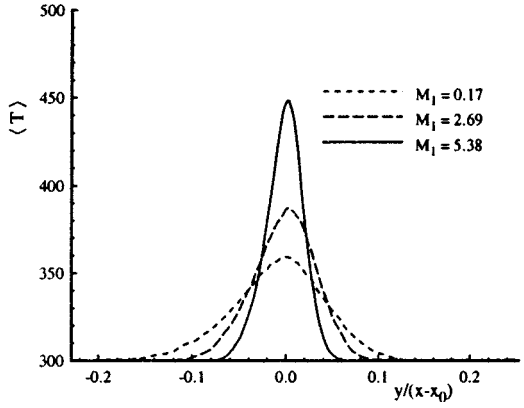

FIG. 7. Effect of increasing Mach number on the mean temperature profiles at the same downstream location.

decreases with increased compressibility. The increased value of the peak temperature can be attributed chiefly to viscous dissipation, which should become more and more important as the Mach number increases, as mentioned in the dimensional analysis. In the case with 8% H_2 in the low-speed stream, the peak temperature is even shifted toward the center of the layer, compared to the low-Mach number case, because of the increased importance of dissipation in the center of the layer.

To prove this point further, an additional calculation has been made, with 1% of reactant in each free stream, and a value of M_1 of 5.38, corresponding to a value of M_2 of 2.16, and of 1.62 for M_c. The result is shown in Fig. 7, along with the low-Mach number results, and the $M_1=2.69$ results. The two trends mentioned above are more pronounced in this plot, the temperature profile becoming both narrower and higher. The temperature rise due to chemical reaction becomes clearly much less important than that coming from fluid dynamical effects, as could be expected.

No treatment of supersonic combustion would be complete without calculations of flows involving discontinuities in the mean fields. Such discontinuities can be artificially introduced[47] to enhance mixing, and it is necessary to be able to predict their effect on the reaction and on the flow. If we consider a shock wave as a region with extremely high mean dissipation rates and/or high mean dilatation rates (in absolute value), we can see that both effects can in theory be accounted for in Eq. (17) (through the terms involving the viscous dissipation and the mean dilatation) for the pressure, and in Eq. (12) (through the terms involving the viscous dissipation and the change in specific volume) for the internal energy. In practice, however, treating discontinuities accurately requires a prohibitive number of particles if one does not know *a priori* the position of the shock. In addition to this problem, the heavy spatial smoothing applied to the mean pressure and described briefly in Delarue and Pope[31] tends to smear out discontinuities in the pressure field. In this respect, the work presented here can only be considered as a first step in extending the applicability of PDF methods to supersonic combustion. Although the issues are mainly numerical, the treatment of discontinuities has to be the subject of subsequent research.

V. CONCLUSIONS

We have presented a new PDF model to calculate the statistics of high-speed turbulent reacting flows. The approach is based on the solution of a modeled evolution equation for the joint PDF of velocity, turbulent frequency, pressure, specific internal energy (or enthalpy), and mixture fraction. The agreement with experimental data at low-Mach number is quite satisfactory, for flows with an equivalence ratio greater than one. The model, however, does not give the correct behavior for flows with an equivalence ratio smaller than one: the flip experiments are not reproduced accurately. The trends exhibited by the behaviour of the re-

sults at higher Mach numbers meet the expectations: the temperature profiles become narrower, with an increased peak value. The turbulence and mixing models incorporated in our formulation are very simple, but it will be straightforward to incorporate more accurate models when they are made available—for example, local mixing models or turbulence models reproducing the effects of compressibility on the pressure–rate of strain correlation.

The approach allows us to deal with flows exhibiting strong continuous spatial variations of the mean pressure, but an accurate treatment of shock waves is, at present, out of reach. Dealing with flows involving discontinuities requires too many particles and a very fine grid to overcome the spatial smearing of pressure discontinuities caused by the smoothing algorithm (which is necessary to eliminate statistical noise). Further improvement of the method is therefore needed in that respect.

The reaction studied in this paper did not call for an accurate treatment of finite-rate chemistry. The approach, however, is general enough to remain unchanged in the case of finite reaction rates or more complicated chemical mechanisms.

ACKNOWLEDGMENTS

This work was supported by Grant NAG 1 1542 from NASA Langley Research Center, Program Manager Dr. Phil Drummond.

APPENDIX: GENERAL EQUATIONS

In the following we present the general PDF formulation, in the case of a mixture of n ideal gases, but without any additional assumptions. In particular, we do not make the simplifications of Eqs. (2) and (3), and we allow for finite reaction rates.

At the stochastic particle level, the thermochemistry is described by the particle pressure p^*, the particle temperature T^* (replacing the particle specific internal energy e^*, which becomes inconvenient when the specific heats vary with temperature), and the particle mass fractions Y_i^*, where i refers to the ith species. It is no longer useful to work with the mixture fraction ξ^* in the case of finite reaction rates.

The evolution equations for the mass fractions Y_i^* can be written as

$$dY_i^* = M_i\, dt + S_i\, dt \tag{A1}$$

In the above equation, M_i is the molecular mixing term and S_i is the reaction source term. In this paper, we have used the IEM model for M_i.[41] The source term S_i does not need to be modeled in a PDF formulation. We can, for example, use Arrhenius' law to compute this term. Hence the extension to finite reaction rates is straightforward.

To obtain the evolution equation for the particle temperature, it is useful to consider first the particle specific internal energy e^*. If we write it as

$$e^* = \sum_{i=1}^{n} Y_i^* \left(\Delta H_{f,i}^0 + \int_0^{T^*} c_{v,i}(T)\, dT \right) = \sum_{i=1}^{n} Y_i^* e_i^*,$$

where e_i^* is the specific internal energy for species i, then we can write the evolution equation for the particle temperature as

$$dT^* = \frac{de^* - \Sigma_{i=1}^{n} e_i^*\, dY_i^*}{\Sigma_{i=1}^{n} Y_i^* c_{v,i}(T^*)}. \tag{A2}$$

In this equation, dY_i^* is given by Eq. (A1), and de^* is given by Eq. (12):

$$de^* = \epsilon\, dt - C_\phi \Omega (h^* - \widetilde{h}) dt - p^*\, dv^*, \tag{A3}$$

where v^* is the particle specific volume, related to p^*, T^*, and Y_i^* by the ideal gas equation of state:

$$v^* = \frac{RT^*}{p^*} \sum_{i=1}^{n} \frac{Y_i^*}{W_i}. \tag{A4}$$

It is legitimate to deduce Eq. (A2) from the evolution equations for the particle specific internal energy and for the particle mass fractions, provided the latter do not involve Brownian motion increments, which is the case in Eq. (A1). If Brownian motion increments were present, the evolution equation for T^* would contain an additional term.

Finally, the evolution equation for the particle pressure p^* can be written as

$$dp^* = p^* (A\, dt + B\, dW), \tag{A5}$$

with A and B given by

$$A = \frac{B^2}{2}\left(1 + \frac{1}{\Gamma^*}\right) + \frac{\epsilon}{c_v^* T^*} - \frac{C_\phi}{c_v^* T^*}\, \Omega (h^* - \widetilde{h}) - \frac{\Sigma_{i=1}^{n} e_i^* (M_i + S_i)}{c_v^* T^*} + \frac{\displaystyle\sum_{i=1}^{n} \frac{M_i + S_i}{W_i}}{\displaystyle\sum_{i=1}^{n} \frac{Y_i^*}{W_i}} - \Gamma^* \left(\frac{\partial \langle U_i \rangle}{\partial x_i} - \Omega_A (p^* - \langle p \rangle) \right), \tag{A6}$$

$$B = \frac{\langle \rho \rangle}{\left\langle \dfrac{p}{\Gamma^*} \right\rangle} \frac{p_e^2}{\tau_a} \frac{1}{\langle \rho \rangle^2 \widetilde{a}^2}. \tag{A7}$$

The quantities c_v^*, Γ^*, and Ω_A are given by

$$c_v^* = \sum_{i=1}^{n} Y_i^* c_{v,i}(T^*),$$

$$\Gamma^* = 1 + \frac{p^* v^*}{T^* c_v^*},$$

$$\Omega_A = -\frac{1}{2\tau_a \langle \rho \rangle \widetilde{a}^2}.$$

The quantities τ_a and p_e are defined in Zeman.[14]

In the case where simplifications (2) and (3) can be made, it is more convenient to work with the specific internal energy than with the temperature. It can be readily verified that, in this case, the expressions for A [Eq. (A6)] and B [Eq. (A7)] simplify to yield Eqs. (17) and (18). Even though the

formulation has been designed for variable specific heats and finite-rate chemistry, the chemistry studied in this paper allowed for those simplifications.

[1] S. K. Lele, ''Compressibility effects on turbulence,'' Annu. Rev. Fluid Mech. **26**, 211 (1994).
[2] N. T. Clemens and M. G. Mungal, ''Large-scale structure and entrainment in the supersonic mixing layer,'' J. Fluid Mech. **284**, 171 (1995).
[3] D. Papamoschou and A. Roshko, ''The compressible turbulent shear layer: An experimental study,'' J. Fluid Mech. **197**, 453 (1988).
[4] M. Samimy and G. S. Elliott, ''Effects of compressibility on the characteristics of free shear layers,'' AIAA J. **28**, 439 (1990).
[5] M. Samimy, M. F. Reeder, and G. S. Elliott, ''Compressibility effects on large structures in free shear flows,'' Phys. Fluids. A **4**, 1251 (1992).
[6] D. Papamoschou, ''Structure of the compressible turbulent shear layer,'' AIAA J. **29**, 680 (1990).
[7] G. S. Elliott and S. Samimy, ''Compressibility effects in free shear layers,'' Phys. Fluids A **2**, 1231 (1990).
[8] S. G. Goebel and J. C. Dutton, ''Experimental study of compressible turbulent mixing layers,'' AIAA J. **29**, 538 (1990).
[9] S. G. Goebel, J. C. Dutton, H. Krier, and J. P. Renie, ''Mean and turbulent velocity measurements of supersonic mixing layers,'' Exp. Fluids **8**, 263 (1990).
[10] S. Sarkar, G. Erlebacher, M. Y. Hussaini, and H. O. Kreiss, ''The analysis and modelling of dilatational terms in compressible turbulence,'' J. Fluid Mech. **227**, 473 (1991).
[11] S. Sarkar, ''The pressure-dilatation correlation in compressible flows,'' Phys. Fluids **4**, 2674 (1992).
[12] S. Sarkar, G. Erlebacher, and M. Y. Hussaini, ''Direct simulation of compressible turbulence in a shear flow,'' Theor. Comput. Fluid Dyn. **2**, 291 (1991).
[13] O. Zeman, ''Dilatation dissipation: The concept and application in modeling compressible mixing layers,'' Phys. Fluids A **2**, 178 (1990).
[14] O. Zeman, ''On the decay of compressible isotropic turbulence,'' Phys. Fluids. A **3**, 951 (1991).
[15] O. Zeman and G. Coleman, ''Compressible turbulence subjected to shear and rapid compression,'' in *Turbulent Shear Flows 8* (Springer-Verlag, Berlin, 1993), p. 283.
[16] R. Abid, ''On prediction of equilibrium states in homogeneous compressible turbulence,'' Technical report, NASA Contractor Report No. 4570, 1994.
[17] S. Sarkar, ''The stabilizing effect of compressibility in turbulent shear flow,'' J. Fluid Mech. **282**, 163 (1995).
[18] P. A. Libby and F. A. Williams, in *Turbulent Reacting Flows* (Springer-Verlag, Berlin, 1980).
[19] P. A. Libby, in *Turbulent Reacting Flows* (Springer-Verlag, Berlin, 1994).
[20] P. E. Dimotakis, ''Turbulent free shear layer mixing and combustion,'' in *High-Speed Flight Propulsion Systems*, edited by S. N. B. Murthy and E. T. Curran (AIAA, Washington, D.C., 1991), pp. 265–340.
[21] S. B. Pope, ''Pdf methods for turbulent reactive flows'' Prog. Energy Combust. Sci. **11**, 119 (1985).
[22] K. N. C. Bray, P. A. Libby, and F. A. Williams, ''High speed turbulent combustion,'' *Turbulent Reacting Flows*, edited by P. A. Libby (Academic Press, New York, 1994).
[23] S. M. Correa and S. B. Pope, ''Comparison of a Monte Carlo pdf/finite-volume mean flow model with bluff-body raman data, in the *24th International Symposium on Combustion* (The Combustion Institute, 1992) p. 279.
[24] G. C. Chang, ''A Monte Carlo PDF/All-speed finite-volume study of turbulent flames,'' Ph.D. thesis, Cornell University, 1995.
[25] S. B. Pope and Y. L. Chen. ''The velocity-dissipation probability density function model for turbulent flows,'' Phys. Fluids **2**, 1437 (1990).
[26] S. B. Pope, ''Application of the velocity-dissipation probability density function model to inhomogeneous turbulent flows,'' Phys Fluids **3**, 1947 (1991).
[27] S. B. Pope, ''Position, velocity and pressure correction algorithm for particle method solution of the pdf transport equations,'' Technical Report NO. FDA 95-06, Cornell University, 1995.
[28] A. T. Hsu, Y.-L. P. Tsai, and M. S. Raju, ''Probability density function approach for compressible turbulent reacting flows,'' AIAA J. **7**, 1407 (1994).
[29] C. Dopazo, Recent developments in pdf methods, in *Turbulent Reacting Flows*, edited by P. A. Libby (Academic Press, New York, 1994).
[30] W. C. Welton and S. B. Pope, ''A pdf-based particle method for compressible turbulent flows,'' AIAA Paper No. 95-0804, 1995.
[31] B. J. Delarue and S. B. Pope, ''Application of pdf methods to compressible turbulent flows,'' Phys. Fluids A **9**, 2704 (1997).
[32] Gmelin, *Handbook of Inorganic Chemistry: F Fluorine Suppl.* (Springer-Verlag, Berlin, 1980), Vol. 2.
[33] M. G. Mungal and P. E. Dimotakis, ''Mixing and combustion with low heat release in a turbulent shear layer,'' J. Fluid Mech. **148**, 349 (1984).
[34] M. W. Chase, C. A. Davies, J. R. Downey, D. J. Frurip, R. A. McDonald, and A. N. Syverud, ''Janaf thermochemical tables,'' J. Phys. Chem. Ref. Data **14** (1985).
[35] A. T. Norris and S. B. Pope, ''Modeling of extinction in turbulent diffusion flames by the velocity-dissipation-composition pdf method,'' Combust. Flame **100**, 211 (1995).
[36] R. W. Bilger, ''Turbulent flows with nonpremixed reactants'' in Ref. 29, Chap. 3, pp. 65–113.
[37] J. C. Hermanson and P. E. Dimotakis, ''Effects of heat release in a turbulent, reacting shear layer,'' J. Fluid Mech. **199**, 333 (1989).
[38] S. R. Turns, *An Introduction to Combustion* (McGraw-Hill, New York, 1996).
[39] D. C. Haworth and S. B. Pope, ''A generalized Langevin model for turbulent flows,'' Phys. Fluids **29**, 387 (1986).
[40] Jayesh and S. B. Pope, ''Stochastic model for turbulent frequency,'' Technical report FDA 95-05, Cornell University, 1995.
[41] C. Dopazo, ''Probability density function approach for a turbulent axisymmetric heated jet. Centerline evolution,'' Phys. Fluids **18**, 397 (1975).
[42] G. Erlebacher, M. Y. Hussaini, H. O. Kreiss, and S. Sarkar, ''The analysis and simulation of compressible turbulence,'' Theor. Comput. Fluid Dyn. **2**, 73 (1990).
[43] J. L. Lumley and H. Tennekes, *A First Course in Turbulence* (MIT Press, Cambridge, 1972).
[44] D. W. Bogdanoff, ''Compressibility effects in turbulent shear layers,'' AIAA J. **21**, 926 (1983).
[45] G. L. Brown and A. Roshko, ''On density effects and large structures in turbulent mixing layers,'' J. Fluid Mech. **64**, 775 (1974).
[46] A. W. Vreman, N. D. Sandham, and K. H. Luo, ''Compressible mixing layer growth rate and turbulence characteristics,'' J. Fluid Mech. **320**, 235 (1996).
[47] A. Kumar, D. M. Bushnell, and M. Y. Hussaini, ''Mixing augmentation techniques for hypervelocity scramjets,'' AIAA J. Prop. Power **5**, 314 (1989).